2010 IEEE International Conference on Robotics and Automation
Anchorage Convention District
May 3-8, 2010, Anchorage, Alaska, USA

Accurate modeling of low-cost piezoresistive force sensors for haptic interfaces

L. Paredes-Madrid, P. Torruella, P. Solaeche, I. Galiana and P. Gonzalez de Santos
Center of Automation and Robotics UPM- CSIC
Ctra. Campo Real; Km 0,2
28500 Arganda del Rey; Madrid; Spain

***Abstract* — In this paper we present a new method for measuring forces using piezoresistive sensors. This method dramatically increases the accuracy and repeatability of the readings compared with traditional methods. These improvements will allow the common use of piezoresistive sensors in robotic applications, where only expensive and sophisticated force sensors such as load cells are currently used. We also present a sketch of a haptic interface under development, consisting of a data glove in which these force sensors are integrated. This interface is intended to control an Intelligent Assist Device by measuring operator-applied forces to the load. The new method proposed for measuring forces in piezoresistive sensors consists of reading conductance and capacitance by applying DC and sinusoidal waveforms to the sensors, thereby allow us to determine a multivariable estimation of force, instead of using the traditional, purely resistive model that has been used up to now.**

I. Introduction

MEASURING force has always been a task of great importance in robotics. The number of robots that work in direct cooperation with humans has increased dramatically over the last ten years [1], [2], [3]. This collaborative human-robot environment requires continuous monitoring of the forces exerted by robots on humans in order to keep those forces within comfortable and safe limits [4]. Many fields of research and applications such as intelligent assist devices [5], haptic interfaces [6], [7], human grip force analysis [8], [9], [10], instrumented gloves [11], [12], footwear design [13], and medical robotics are seeking solutions for measuring force. As a general rule, the ideal sensor for measuring force must have the following characteristics: high repeatability of readings, small size, light weight, increased robustness and reliability, low drift, low cost, and independent readings of temperature and magnetic field.

In the early stages of robotics, force was measured by installing strain gauges on a robot's links [14]. A Wheatstone bridge made of strain gauges provided a reliable, small, and non-invasive method for measuring deformation, then the forces applied to the robot's links could be deduced from Young's modulus of material and the link's dimensions. This method is still used, but it must be noted that a flexible element is required to achieve a variation of resistance. In some applications, material deformation is measured by light intensity on optical fibers [15].

Load cells are another type of force sensor. They are typically used in applications that require force measurement on several axes and that require high repeatability, high robustness, and low drift. Unlike strain gauges, they do not need to be mounted on a bendable surface and are available in many sizes, depending on the range of forces they can withstand.

The major drawbacks of load cells are their volume and weight, which make them unsuitable for use in some applications, such as studying human grip force and haptic interfaces. These applications require the least invasive methods available for measuring force. Piezoresistive sensors are the best solution, since they are light-weight, thin, and small. They can be fashioned to fit inside a data glove [10] or in a human joint, such as a knee [16] or an elbow, and they are also inherently safe because they are passive. However, piezoresistive force sensors offer significantly lower repeatability than load cells, and they exhibit considerable hysteresis and drift. These undesirable characteristics limit the use of these sensors to applications that do not need to be highly accurate [4], but the reduced price of piezoresistive sensors compared with load cells is generating an increase in use and research interest.

In this paper, we compared two prior studies on the most widely used piezoresistive force sensors [17], [18]. Previous studies performed by Lebossé et al. [4] and Vecchi et al. [19] show the comparative behavior of both sensors. We chose FlexiForce sensors for our study, because the manufacturer has developed many specific task sensors [13], [16] used in several research and industrial applications.

A new type of haptic interface [20], under development, is being designed to control an Intelligent Assist Device (IAD) that requires non-invasive force measurement. This control interface consists of a data glove with a 3DOF Orientation Device (yaw, pitch, and roll), which is based in an Inertial Measurement Unit (IMU) and a force measurement system installed in the palm-side of the glove.

As an operator uses his hand to push a load carried by the IAD, the haptic glove measures the forces, thereby generating a vector magnitude, and depending on the IMU readings, consequent direction is given to the force vector. The IAD motion is controlled by this force vector, and therefore an amplification of operator's force is obtained without using joysticks, buttons, or handles. An overview of the haptic glove is depicted in Fig.1

Since high correspondence is desired between the forces exerted by the operator and the consequent IAD motion, every force contribution must be accurately measured in order to achieve high colinearity and a proportional response. However, piezoresistive sensors such as FlexiForce sensors are not accurate enough, and therefore a new method for reducing force estimation errors is required. Note that inherently accurate force sensors, such as load cells, are unsuitable for a haptic glove due to their bulk.

In this paper, we develop a new method for reducing force estimation errors in FlexiForce sensors (model A201-100) with a range from 0 to 450 N. This method implies formulating an electrical model for the sensor in terms of passive components such as resistors (R), inductors (L), and capacitors (C).

To determine inductance and capacitance variation along force changes, sinusoidal waveforms must be applied to the sensor. This is the most innovative aspect of this study, and

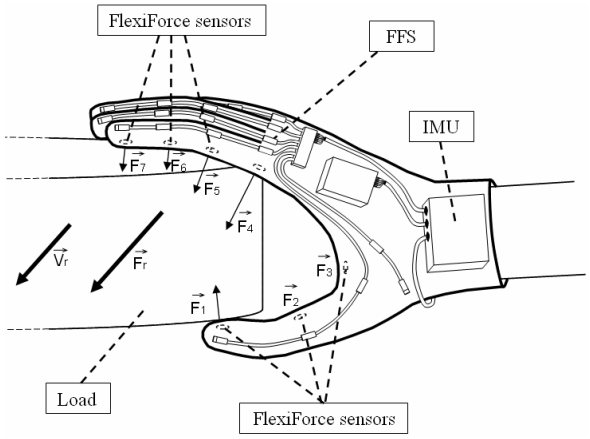

Fig. 1: Sketch of the haptic glove under development. Note that FlexiForce sensors are installed on the palm-side of the glove, while the IMU and the Finger Flexion Sensors (FFS) are installed on the dorsal-side of the glove. The force contributions generated by each sensor (F_1 ~F_7) are totaled to obtain a resulting Force (Fr) and consequently a resulting Velocity (V_r) for the load and the IAD.

it will allow us to devise a new, multivariable estimation of force, instead of using the traditional, purely resistive conductance model proposed by the manufacturer [17]. A large number of sensors were used for this study to obtain a valid generalization of results.

This paper is organized as follows: Section II describes a procedure for obtaining an electrical model of FlexiForce sensors in terms of resistance, capacitance, and inductance. Sections III and IV show the experimental set-up and the results obtained when applying sinusoidal waveforms to eight sensors according to force changes from 0 to 250 N, including sensor frequency response. Section V presents a series of empirical models, based on conductance and capacitance changes in FlexiForce sensors as a function of force. Finally, the conclusions are presented, and future work is discussed.

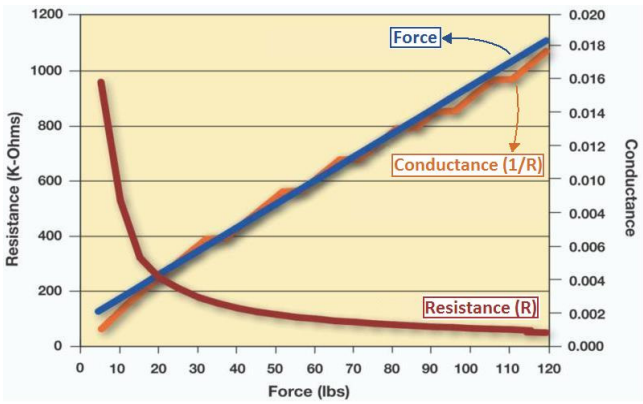

Fig. 2: Typical variation of resistance and conductance, and a fit curve for an A201-100 FlexiForce Sensor (Image taken from a Tekscan White Paper: Free Sensors for design. The image legend was modified for better comprehension).

II. Sensor Electrical Model

The typical response of an A201-100 FlexiForce sensor in terms of resistance and conductance according to force changes is shown in Fig. 2. Note that the conductance curve in Fig. 2 shows step changes. Resistance changes hyperbolically as force increases. Since a linear response is desired, the circuit introduced in [17] is used, thereby allowing us to obtain a linear conductance variation when an input DC signal is applied. This method is traditionally used for measuring forces in piezoresistive sensors [4], [9], [11], [17], [19].

To obtain an RLC sensor model, the circuit introduced in [17] was modified as in Fig. 3, including a three-position selector for switching between three input signals:

$$V_{s1} = -5V \tag{1}$$

$$V_{s2} = A_s \sin\left(2\pi f t\right) \tag{2}$$

$$V_{s3} = A_s \sum_{K=0}^{\infty} \left[u(t-KT) - u(t-t_d-KT)\right] - \frac{A_s}{2} \tag{3}$$

where f and A_s are the signal frequency and amplitude, respectively; FSR in Fig. 3 is the FlexiForce sensor under study; $t_d = 1/\left(2f\right)$ is the time delay in V_{s3} (3); and $u(t)$ is the unity step function. Therefore, (3) is a square wave with frequency f, amplitude A_s, and a duty cycle of 50%.

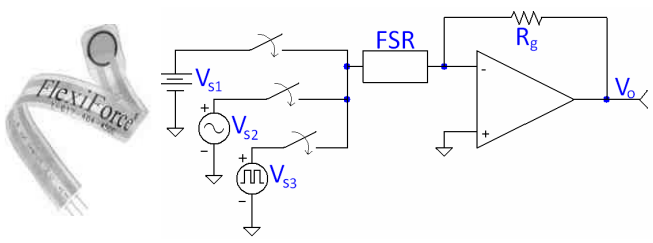

(a) (b)

Fig. 3: (a) Picture of a FlexiForce Sensor. (b) Linearization circuit for FlexiForce sensors (FSR) with multiple input signals.

The transfer function of the inverting amplifier of Fig. 3 is given by the following:

$$Vo = -\left(R_g / Z_{FSR}\right)Vs \qquad (4)$$

where Z_{FSR} is the impedance of the FlexiForce sensor and R_g is a pure resistor used for controlling the amplifier gain.

When signal V_{s2} (2) was selected, a phase shift of -180º was observed at the output voltage (V_o) when operated at a very low frequency. As the frequency was increased up to a few Megahertz, the phase shift decreased to a minimum of -90º, thereby considering the minus sign in the amplifier transfer function (4), which caused a -180º phase shift. The phase shift due to Z_{FSR} is therefore 90º. This essential clue allowed us to formulate a first order resistor-capacitor (RC) model for the FlexiForce sensors. An electrical model including inductance is not possible since the phase shift introduced by the FlexiForce sensor is always positive. Note that the sensor's capacitance introduces a zero into the system, thereby causing positive phase shifts, as discussed in Section IV.

There are two possible variants for a first order RC circuit: RC series or RC parallel (see Fig. 4). To identify the proper model for the sensor under study, signal V_{s3} (3) was selected as the input in the circuit of Fig. 3. When plotting

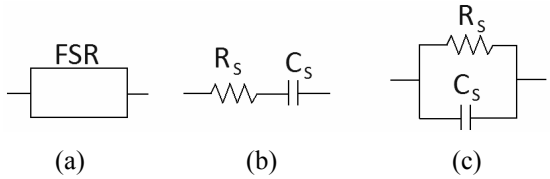

Fig. 4: Possible electrical models of the FlexiForce sensor. (a) Black box model. (b) RC series model. (c) RC parallel model.

the experimental results obtained for V_o and V_{s3} (3) in Fig. 5, ringing was observed in V_o. The ringing occurred due to current spikes flowing through the sensor. This response is typical of an RC parallel circuit (see Fig. 4c), but it is not possible in an RC series circuit (see Fig. 4b): since the series resistor (R_s) in Fig. 4b limits the peak current, the ringing would not appear.

Another way to discard the RC series as the FlexiForce model is to apply V_{s1} (1) as the input signal to the circuit of Fig. 3. An RC series model would not allow Direct Current (DC) to flow through the sensor because of the capacitor effect (C_s), and V_o would therefore be zero. However, an output voltage was observed experimentally, so the premise of an RC series model was incorrect.

III. Experimental Set-Up

Since the RC parallel electrical model was a fit for the response of the FlexiForce sensors, a test bench for studying force effects on conductance and capacitance was built (see Fig. 6). The test bench could handle up to eight sensors simultaneously. An interleaved configuration was used by placing a puck between adjacent sensors. The puck's weight was negligible due to the low density of the material used;

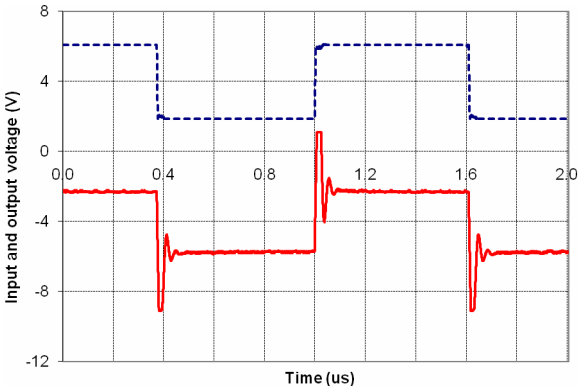

Fig. 5: Sensor output response, V_o (red solid line), to a square wave input, V_{s3} (dashed blue line).

this was important, because we wanted to load every sensor with the same weight. Forces were generated by placing calibrated weights on the pack of sensors.

The test bench could apply a maximum force of 250 N to the pack of sensors. This force is equal to half of the range of the A201-100 FlexiForce sensor. The force step was 5 N, so a total of 50 different forces were generated during the experiment.

A differential equation for the circuit in Fig. 3 could be obtained by replacing FSR in (4) with an RC parallel configuration. The following Equation will let us study the variation in resistance, R_s, and capacitance, C_s, along force changes.

$$\frac{V_{s2}}{R_s} + C_s \frac{dV_{s2}}{dt} = -\frac{V_o}{R_g} \qquad (5)$$

We chose V_{s2} (2) as the input signal in (5) for the following reasons: First, formulating expressions for C_s and R_s when using (2) as the input allowed us to use phase shift and output amplitude measurements, which were easier to

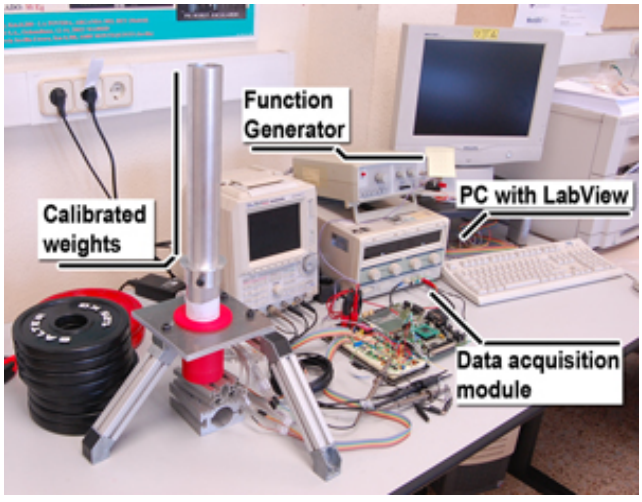

Fig. 6: Test bench overview. Most relevant parts are marked with arrows.

acquire than the maximum peak and the ringing frequency when (3) was used as the input. Second, the input signal V_{s3} (3) generated excessive and very noisy ringing in the output shape that the sensor could not withstand for extended periods of time. The input signal V_{s3} (3) was suitable only for identification purposes but not for continuous operation. Finally, it is impossible to perform capacitance measurements by applying a DC signal such as V_{s1} (1), so it had to be discarded. Solving (5) for V_{s2} allowed us to obtain the following expression for V_o:

$$V_o = -A_s R_g \left(\frac{\sin(2\pi ft)}{R_s} + 2\pi f C_s \cos(2\pi ft) \right) \qquad (6)$$

Equation (6) can be rewritten as a sine function with a phase shift (ϕ) as:

$$V_o = A_o \sin(2\pi ft + \phi) \qquad (7)$$

Joining (6) and (7) results in:

$$R_s = \frac{R_g A_s}{A_o \cos(\phi)} \quad (8) \quad \text{and} \quad C_s = \frac{A_o \sin(\phi)}{R_g A_s 2\pi f} \qquad (9)$$

where the output amplitude (A_o) and the phase shift (ϕ) were measured experimentally for every exerted force. Note that f, R_g, and A_s were already known.

In order to automate the process of measuring the phase shift (ϕ) and the output amplitude (A_o) for the sensors, a modified version of the circuit in Fig. 3 is shown as a block diagram in Fig. 7. Two analog switches (ADG441) were used to select only one sensor at a time. A switch was also used to select between the sinusoidal input, V_{s2} (2), and the DC input, V_{s1} (1). This will be useful for comparing the results obtained from the newly proposed method with the traditional conductance model.

Conditioning of the phase shift readings was performed using two comparators: an XOR logic gate and a low pass filter. The output amplitude was converted to a DC value by a precision rectifier circuit. A superdiode configuration was therefore used with DC filtering. A microcontroller (DSPic30F) controlled the activation of analog switches for the sensors and inputs, and it also digitized the phase shift and output amplitude readings using an ADC converter. This data was sent to a PC for post- processing and analysis.

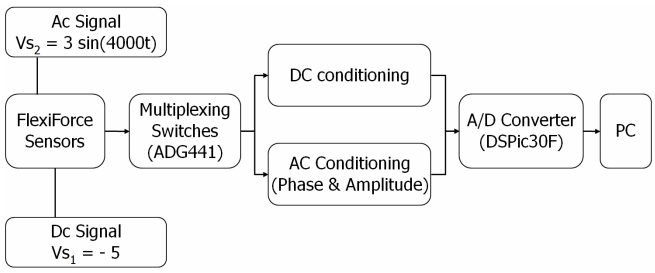

Fig. 7: Block diagram of the final circuit for measuring up to eight sensors simultaneously.

IV. Sensor Response Along Force Changes

A. Determination of parameters for sinusoidal input signals

It was necessary to determine an adequate set of parameters for the input signal (2), wherefore A_s and f had to be chosen so that the sensor model was valid for any applied force. This implied that the sensor's response had to correspond to equations (8) and (9). The input amplitude, A_s, had to avoid sensor overloading by limiting the sensor current to less than 2.5 mA, as recommended in [17]. Considering that the lowest sensor resistance, R_s, is obtained at the maximum force (Fig. 2), A_s was tuned according to this condition.

Choosing an adequate frequency value, f, was rather complicated due to the fact that nonlinear effects appear as the frequency is increased. A phase bode plot of the sensor depicted in Fig. 8 shows the experimentally measured phase shift (ϕ) and the expected phase shift. The expected phase shift expression is built up by joining (8) and (9) as follows:

$$\phi = \arctan(2\pi f C_s R_s) \qquad (10)$$

The values of R_s and C_s used in (10) were measured at a very low frequency, where the sensor had a linear response. Figure 8 shows that both phase shift curves (experimentally measured and expected) are quite similar until reaching a certain frequency, which we called the divergent frequency. The divergent frequency was the frequency where the RC parallel model described up to now was no longer valid.

The divergent frequency changed from one sensor to other, depending on the force applied to the sensor. We deliberately chose 125 N as the applied force in Fig. 8, because this value was equal to half the maximum exerted force during all experiments.

A detailed study of the divergent frequency along force changes was beyond the scope of this article. However, we had to choose an input frequency in (2) that was reasonably smaller than the divergent frequency but high enough to

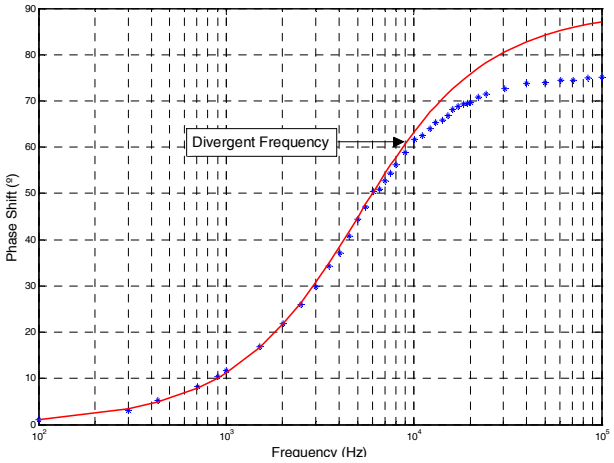

Fig. 8: Phase Bode Plot of the FlexiForce sensor. Experimentally measured phase shift (asterisk) and expected phase shift (solid line).

produce noticeable phase shifts as the force changed. In practice we used $A_s = 3V$ and $f = 4\,KHz$.

B. Variation of conductance and capacitance along force changes

The typical values of C_s for the eight sensors measured using the circuit of Fig. 7, the input signal V_{s2} (2), and expressions (7) and (9) were 100-250 pF when unloaded and 700 pF-900 pF when 250 N was applied to the sensor. This means that the sensors exhibited a piezocapacitive behavior. The piezocapacitive property of the FlexiForce sensors had been unknown up to now, and only the piezoresistive property of the sensor had been used for estimating forces [4], [6], [9], [11], [17], [19]. Figure 9 shows the variation of C_s and V_o for a given sensor. Note that the curves are linear, but they both exhibit considerable step changes as in Fig. 2.

The main contribution of this paper consists in using this piezocapacitive property to reduce force estimation errors, given that additional information on the applied forces that can be found in sensor capacitance.

V. Multivariable Sensor Modeling

To reduce force estimation errors in measurements of FlexiForce sensors, we have developed four empirical models based upon conductance and capacitance changes.

The first one is the traditional conductance model obtained when V_{s1} (1) is selected as the input in the circuit of Fig. 7. This method will be used as a reference for further comparison. The second model is a linear regression of the capacitance values, so input V_{s2} (2) is chosen as the input in the circuit of Fig. 7, and then expressions (7) and (9) are used for estimating C_s. The third model consists of averaging the output forces predicted by the first and second models.

The fourth model is a feedforward neural network with two inputs (V_o and C_s), one hidden layer with two neurons, and one neuron output. The same network topology was used for all sensors but training data was taken individually for each sensor; this is necessary because capacitance is different from one sensor to other as stated previously in Section IV-B. The neural network was trained offline.

We trained the neural network with V_o, obtained when using both (1) as the input in the circuit of Fig. 7 and when using (2) as the input. In practice, slightly better results were obtained when using (1) as the input rather than (2), because the V_o values were more repeatable.

The histogram in Fig. 10 summarizes the experimental results for each sensor in terms of the mean squared error for the four models under study.

An important set of facts can be concluded from Fig. 10. First, the capacitance model generated lower errors than the traditional conductance model for all sensors. This is an important fact, because it shows that capacitance readings are more repeatable than conductance measurements.

Second, averaging the predicted forces from the conductance and capacitance always reduced MSE when compared with traditional conductance model.

Third, the neural network model was the best technique for reducing output errors. This method worked better than the others due to the fact that a two-variable function is built from the V_o and C_s values. Conversely, the other three methods only take into account one of the two variables at any given time. Averaging the predicted forces from the conductance and capacitance models seldom produced better results than the neural network model (which was the case with sensor 1, but not the other sensors).

A 3D plot of the surface generated by the neural network for a given sensor is depicted in Fig. 11. An arrow superimposed on the surface indicates the typical variation of V_o and C_s as force increases. When either V_o or C_s values deviate from the ideal trajectory described by the white arrow, force is estimated incorrectly. However, the soft surface generated by the neural network tends to mitigate this error and improve sensor response.

Finally, the traditional conductance model produced output errors that were notably different from one sensor to another. These imbalances are a frequent source of problems in applications in which several sensors are used [6]. Table 1 summarizes the improvements introduced by the neural network, compared with the traditional conductance model for the eight sensors under study.

Note that the neural network model reduces MSE dispersion to a narrow range of 0.107 – 0.515, whereas the dispersion of the traditional conductance model is noticeable higher 0.258- 2.01. The percentage of error reduction is computed (PER) from:

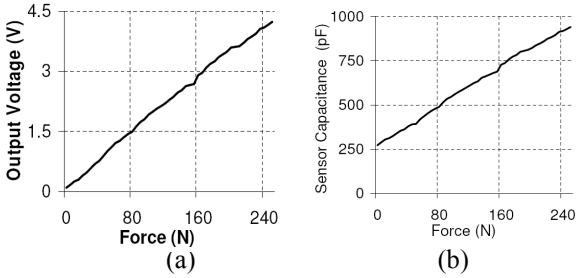

Fig. 9: Variation of V_o and C_s along force changes. (a) Variation of V_o when V_{s1} (1) is selected as the input. (b) Variation of C_s when V_{s2} (2) is selected as the input.

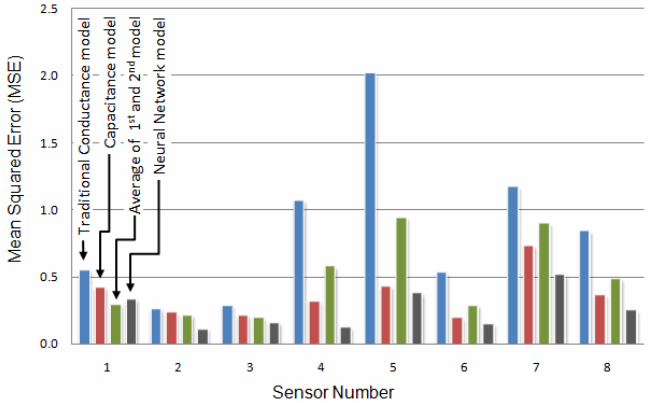

Fig. 10: Mean Squared Error of the four models proposed for the eight sensors under study.

TABLE I
COMPARISON OF TRADITIONAL CONDUCTANCE MODEL WITH NEURAL NETWORK MODEL IN TERMS OF MEAN SQUARED ERROR (MSE)

Sensor	1	2	3	4	5	6	7	8
MSE of traditional conductance model	0.547	0.258	0.285	1.06	2.01	0.527	1.17	0.839
MSE of neural network model	0.330	0.107	0.156	0.118	0.374	0.145	0.515	0.249
Percentage of error reduction (%)	39.7	58.2	44.9	88.8	81.4	72.4	55.9	70.2
Average Percentage of error reduction								64%

$$\text{PER} = \left(1 - \frac{\text{MSE neural network model}}{\text{MSE traditional conductance model}}\right) \quad (11)$$

A high value of PER for a given sensor means that the neural network model has substantially reduced estimation error compared with the traditional conductance model. An average of these values for the eight sensors under study was also computed, resulting equal to 64%.

VI. CONCLUSIONS AND FUTURE WORK

An equivalent RC circuit of FlexiForce sensors was presented. A piezocapacitive property was found in these sensors, and a two-variable model of force estimation was developed, which reduced the mean squared error in 64% when compared with the traditional conductance model. This feature is of paramount importance for the efficient use of FlexiForce sensors in robotics applications and haptic gloves.

Future work will focus on determining force effects on the divergent frequency and will focus on proposing better and more accurate sensor models that help to reduce force estimation errors. A comparative study in terms of the associated complexity between the traditional conductance model and the multivariable model is also pending.

VII. ACKNOWLEDGMENTS

This work has been funded by the Spanish Ministry of Science and Innovation through grant DPI2007-65728.

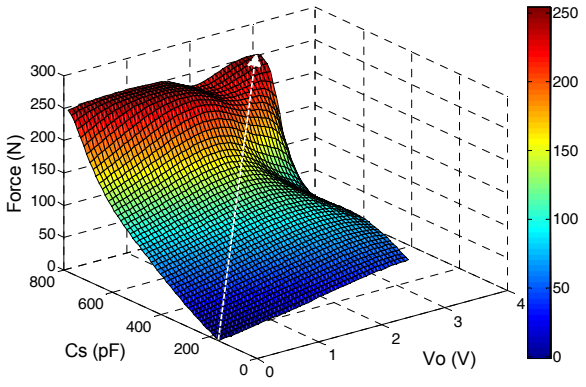

Fig. 11: 3D plot of the surface generated by the neural network for predicting forces applied to FlexiForce sensors. An ideal variation of V_o and C_s as force increases is indicated by a white arrow.

REFERENCES

[1] M. A. Peshkin, J. E. Colgate, W. Wannasuphoprasit, C.A. Moore, R.B. Gillespie, P. Akella. "Cobot Architecture", in *IEEE Transactions on Robotics and Automation*, vol. 17, pp. 377-390, August 2001.

[2] M. Van Damme, F. Daerden, D. Lefeber. "A Pneumatic Manipulator used in Direct Contact with an Operator", in *IEEE International Conference on Robotics and Automation*, (Barcelona, Spain), pp.4494-4499, April 2005.

[3] J.E. Colgate, M.A. Peshkin, J. Santos-Munné, A. Makhlin, P.F. Decker, S.H. Klostermeyer. "Control Handle for Intelligent Assist Devices", U.S. Patent No. 6,738,691, May 2004.

[4] C. Lebossé, B. Bayle, M. de Mathelin, P. Renaud. "Nonlinear modeling of low cost force sensors", in *IEEE International Conference on Robotics and Automation,* (Pasadena, CA, USA), pp. 3437-3442, May 2008.

[5] D. McGee, P. Swanson. "Method of Controlling an Intelligent Assist Device", U.S. Patent No. 6,204,620, March 2001

[6] M. Monroy, M. Ferre, J. Barrio, V. Eslava, I. Galiana. "Sensorized Thimble for Haptics Applications", in *IEEE International Conference on Mechatronics.* (Málaga, Spain), pp.1-6, April 2009.

[7] Z. Ye, G. Auner. "Haptic Interface Prototype for Feedback Control on Robotic Integration of Smart Sensors", in *IEEE International Conference on Control Application,* pp. 995-1000, 2003.

[8] K. N. Tarchanidis, J.N. Lyngouras, "Data Glove With a Force Sensor", in *IEEE Transactions on Instrumentation and Measurement*, vol. 52, pp. 984-989, June 2003

[9] M.C.F. Castro, A. Cliquet, Jr. "A Low-Cost Instrumented Glove for Monitoring Forces During Object Manipulation", in *IEEE Transactions on Rehabilitation Engineering*, vol. 5, pp. 140-147, June 1997

[10] J-H. Lee, Y-S Lee, S-H Park, M-C Park, B-K Yoo, S-M In, "A Study on the Human Grip Force Distribution on the Cylindrical Handle by Intelligent Force Glove (I-Force Glove)", in *International Conference on Control, Automation and Systems*.(Seoul, Korea), pp. 966-969, October 2008.

[11] H. Kazerooni, D. Fairbanks, A. Chen, G. Shin. "The Magic Glove", in *IEEE International Conference on Robotics and Automation*, (New Orleans, LA), pp. 757-763, April 2004

[12] L. Dipietro, A. M. Sabatini, P. Dario, "A Survey of Glove-Based Systems and their Applications", in *IEEE Transactions on Systems, Man, and Cybernetics*, vol. 38, pp. 461-482. July 2008.

[13] J. H. Ahroni, E. J. Boyko, R. Forsberg, "Reliability of F-Scan In-Shoe Measurements of Plantar Pressure" in *Foot and Ankle International*, 9,10 pp. 668-673. October 1998

[14] R. Luo, "A Microcomputer-Based intelligent sensor for Multiaxis Force/Torque Measurement", in *IEEE Transactions on Industrial Electronics*, vol. 35 pp. 26-30. February 1998.

[15] D. Chapuis, R. Gassert, L. Sache, E. Burdet, H. Bleuler, "Design of a simple mri/fmri compatible force/torque sensor", in *IEEE International Conference on Intelligent Robots and Systems*, vol. 3, (Sendai, Japan), pp. 2593-2599, September 2004.

[16] J. L. Pavlovic, Y. Takahashi, J. E. Bechtold, R. B. Gustilo, and R.J. Kyle, "Can The Tekscan Sensor Accurately Measure Dynamic Pressures In The Knee Joint?", in *17th Annual Meeting, American Society of Biomechanics,* October 1991.

[17] Tekscan Inc, FlexiForce User Manual, Available in: http://www.tekscan.com/pdfs/FlexiforceUserManual.pdf, September 2009.

[18] Interlink Electronics, Standard Specification Sensors, Available in: http://www.interlinkelectronics.com/force_sensors/products/forcesensingresistors/standardsensors.html?specs=1, September 2009.

[19] F. Vecchi, C. Freschi, S. Micera, A. Sabatini, and P. Dario, "Experimental evaluation of two commercial force sensors for applications in biomechanics and motor control." In *International Functional Electrical Stimulation Society (IFESS)*, (Aalborg, Denmark), June 2000.

[20] L. Paredes-Madrid and P. Gonzalez-de-Santos, "System and procedure for controlling manipulators", Patent Nº P200930173, Spanish Office of Patents, 2009.